Bulletin of Earthquake Engineering
https://doi.org/10.1007/s10518-024-01958-1

ORIGINAL ARTICLE

Testing the applicability of ground motion prediction equations for the Hainaut region (Belgium) using intensity data

Kris Vanneste[1] · Ben Neefs[1,2] · Thierry Camelbeeck[1]

Received: 17 November 2023 / Accepted: 12 June 2024

Abstract

In regions where strong earthquakes occurred before the deployment of dense seismic and accelerometric networks, intensity datasets can help select appropriate ground motion prediction equations (GMPEs) for seismic hazard studies. This is the case for the Hainaut seismic zone, which was one of the most seismically active zones in and around Belgium during the twentieth century. A recent reassessment of the intensity dataset of the area showed that intensities in this region attenuate much faster with distance than in other parts of northwestern Europe. Unfortunately, this characteristic has not yet been taken into account in current hazard maps for Belgium and northern France. Based on this dataset, we evaluate the goodness of fit of published GMPEs with intensities in Hainaut by means of a ground-motion-to-intensity conversion equation (GMICE) and according to different metrics (Likelihood, Log-likelihood and Euclidean-based Distance Ranking) published in literature. We also introduce a new measure to specifically evaluate the distance trend. Our results show that none of the tested GMPEs convincingly fits the intensity dataset, in particular the fast attenuation with distance. Nevertheless, applying the few GMPEs that show a reasonable fit in seismic hazard computations, we observe a decrease of the influence of the Hainaut seismicity on hazard maps for Belgium and northern France. This result is compatible with the earthquake intensity observations for the last 350 years in this part of Europe.

Keywords Earthquake ground motion · Macroseismic intensity · Goodness of fit · Induced seismicity

✉ Kris Vanneste
kris.vanneste@oma.be

1 Royal Observatory of Belgium, Brussels, Belgium

2 Institute of Mechanics, Materials and Civil Engineering, Université Catholique de Louvain, Louvain-la-Neuve, Belgium

1 Introduction

In Belgium and surrounding areas, the Hainaut region is one of the most seismically active zones (Fig. 1), after the Roer Valley Rift System, where seismicity is linked to known active faults, and the Eastern Ardennes, where the largest historical earthquake in NW Europe occurred in 1692 (Alexandre et al. 2008). As a result, this comparatively small area stands out on most seismic hazard maps made during the past two decades. However, seismicity in Hainaut only started at the end of the nineteenth century and seems to have declined gradually since the late twentieth century (Fig. 2). Historical earthquakes are not known in this area. This evolution is very similar to the history of industrial coal mining in the area, which started becoming significant in the nineteenth century, culminated in the twentieth century and ceased between 1970 and 1984, suggesting that at least part of the Hainaut seismicity may be mining related (triggered or induced). This seismicity is characterized by low to moderate magnitudes, up to $M_W = 4.1$, but due to their shallow focal depth (< 6 km), many earthquakes caused damage with corresponding maximum intensities up to VII, as indicated by a recent synthesis of all available macroseismic observations (Camelbeeck et al. 2022). The reassessment of intensity data on the EMS-98 scale (Grünthal et al. 1998) also showed that intensities in this region attenuate much faster with distance than in other parts of Belgium and NW Europe: at a distance of 30 km, intensities generated by earthquakes in the Hainaut area generally decrease by about 4 degrees with respect to the epicentral intensity I_0, whereas elsewhere in Belgium intensities decrease by only 1 degree over the same distance.

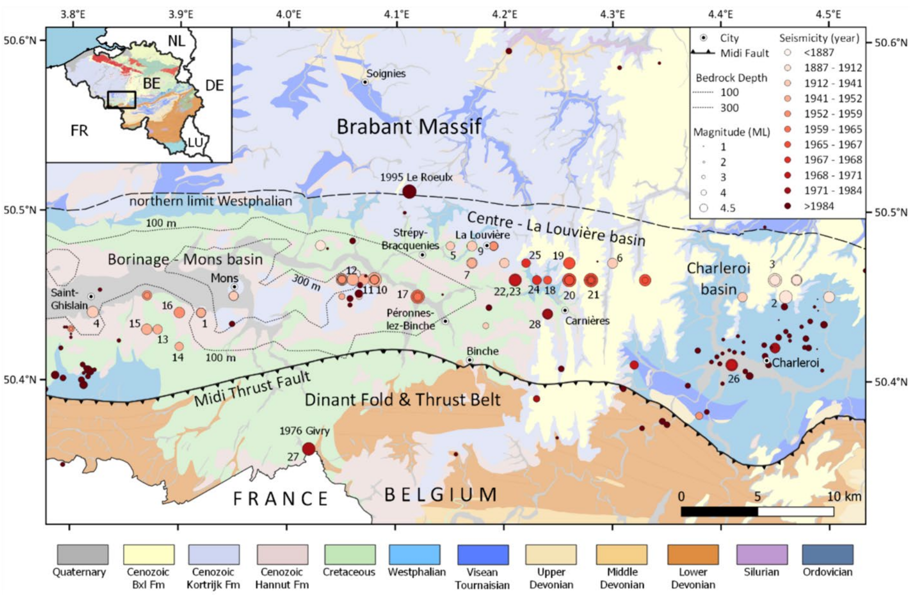

Fig. 1 Map of the Hainaut area in SW Belgium (see inset for location), showing earthquake epicentres (colour-coded by time) and main geological units. Numbers indicate earthquakes with macroseismic data used in this study (see Table 1). The Hainaut coal basin is bounded by the Midi Thrust fault in the south and the northern limit of the Westphalian in the north

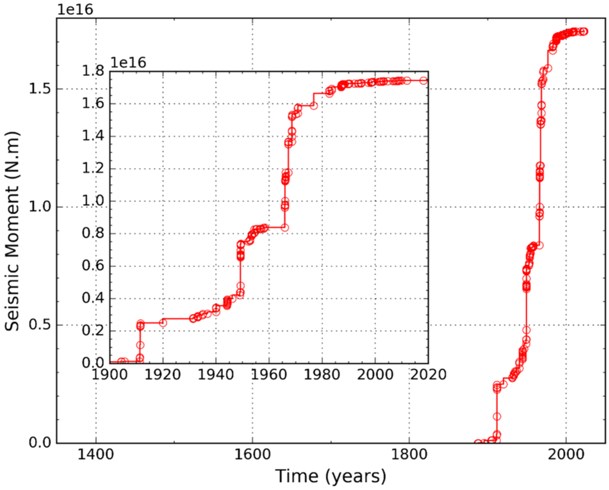

Fig. 2 Evolution of cumulated seismic moment due to earthquakes in the Hainaut area since the start of the historical catalogue in the middle of the fourteenth century. Inset shows the same evolution since the beginning of the twentieth century

Comparison of maps of maximum intensity due to events in the Hainaut zone and due to seismic sources outside the Hainaut area (Fig. 3) shows that the former have caused relatively high intensities, but only inside the Hainaut coal basin, whereas everywhere outside this basin the maximum intensities are related to other earthquakes. This led Camelbeeck et al. (2022) to suggest that the contribution of the Hainaut seismicity to current hazard evaluations is likely overestimated, at least outside the Hainaut coal basin. Those hazard maps (Leynaud et al. 2000; Woessner et al. 2015) are computed using the same ground-motion prediction equations (GMPEs) in Hainaut as in the other seismic zones in and around Belgium and hence do not take into account the observed strong differences in the attenuation of intensity with distance. This highlights the importance of selecting more appropriate GMPEs related to the Hainaut zone, which is the main objective of this study. This is not only useful for seismic hazard assessment (SHA), but also for generating realistic ShakeMaps (Wald et al. 2022) in case of future earthquakes in this region.

In this paper, we first describe the intensity dataset and briefly present the context of the Hainaut seismicity in the frame of seismic hazard assessment. Second, we present the methodological background used to characterize the goodness of fit of GMPEs with respect to intensity data. Next, we select a number of published GMPEs for testing and present the ranking results. Finally, we compute seismic hazard for the wider Hainaut region using the GMPEs showing the best agreement with the intensity dataset and compare the new hazard maps with maps based on our classical selection of GMPEs for stable shallow crust.

2 Dataset

Our dataset consists of macroseismic intensity data points (IDPs) extracted from the traditional macroseismic database of the Royal Observatory of Belgium (ROB) for 28 earthquakes with magnitudes ranging between $M_W = 2.8$ and $M_W = 4.1$ which occurred between 1911 and 1982 in the Hainaut region, as well as the $M_W = 4.6$ Liège earthquake of 1983, which also occurred in a coal mining area with a geological configuration very similar to the Hainaut region. This dataset is the result of a recent compilation by Camelbeeck et al. (2022), which has been further improved. The most significant difference is an update

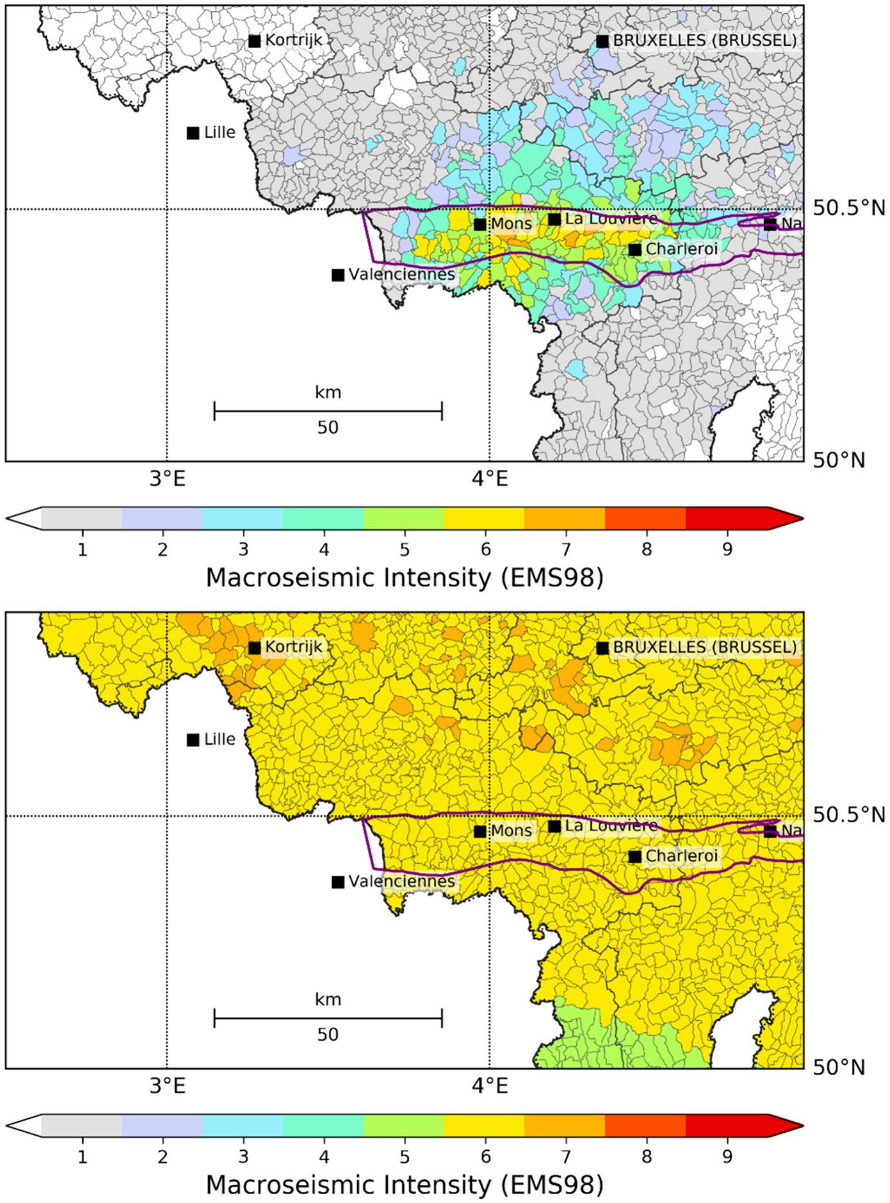

Fig. 3 Comparison of maximum observed intensities in Belgian communes due to earthquakes inside the Hainaut area (top) and due to historical and instrumentally recorded earthquakes outside the Hainaut area (bottom). Purple polygon outlines Hainaut coal basin

of the coordinates of several Belgian localities that are used to locate the IDPs, resulting mainly in insignificant changes (<1 km difference for 96% of the IDPs used here), but a few outliers up to a difference of 22 km occur as well. This can result in significantly higher or lower epicentral distances for a few IDPs. Other adjustments to the data, such as the addition of intensity 1 values (not felt) and the removal, addition or modification of some IDPs (>20 IDPs in total) are negligible in the scope of this study. For the 1983 Liège earthquake, however, more significant changes were made to the IDP dataset as part of a major update of the ROB traditional macroseismic database, such as the addition of 297 new IDPs (~90% not felt), the modification of intensity values of 19 IDPs and the removal of 3 IDPs that were previously assigned to the wrong municipality.

Each IDP consists of a minimum and maximum intensity evaluation, which we averaged for our calculations, and attributed to a location (mostly corresponding to commune centres). We only selected IDPs situated inside a polygon outlining the coal basin (see Fig. 1) or at epicentral distances less than 20 km in the case of the 1983 Liège earthquake, resulting in a total of 1553 IDPs. In addition, Camelbeeck et al. (2022) reassessed epicentral locations and focal depths from the spatial IDP distribution. For all earthquakes, local magnitudes have been determined according to the Belgian M_L scale (Camelbeeck 1985). The moment magnitudes of 17 earthquakes were re-evaluated by Camelbeeck et al. (2022). For the remaining 11 earthquakes, M_W was estimated using the empirical relationship between M_L and M_W established from the calibration earthquakes. The main source parameters of the selected earthquakes, along with the number of IDPs and maximum intensities, are summarized in Table 1; maps of IDPs for each earthquake can be found in Camelbeeck et al. (2022).

3 Current issues in assessing hazard related to Hainaut seismicity

Seismic activity in the Hainaut region is of great concern for seismic hazard assessment in the border area between France and Belgium (Drouet et al. 2020; Leynaud et al. 2000; Martin et al. 2002; Vanneste et al. 2014), and hence for the definition of reference acceleration values in the Belgian and French national annexes to the upcoming revision of the Eurocode-8 building code. For the current hazard maps, two different aspects of this seismicity deserve specific research. First, the origin of this seismicity continues to be unresolved and controversial (Descamps 2009; Troch 2018). In hazard computations, natural seismicity is assumed to be a long-term stationary process, whereas seismicity induced by mining represents only a (past) transient phenomenon. Hence, a reinterpretation of the origin would strongly modify its contribution to the seismic hazard. Second, in contrast to the observed strong intensity decay of these earthquakes, partly caused by their shallow focal depths but also by a stronger attenuation in the upper crust (Camelbeeck et al. 2022), the influence area of the Hainaut seismicity seems to be overextended in the hazard maps (Fig. 4). This inconsistency results from the use of GMPEs that are not appropriate for the specific seismic attenuation characteristics of the Hainaut zone. In this investigation, we focus on this second aspect and develop a methodology to evaluate what are the most appropriate GMPEs to use among the numerous published ones. Considering that the shallow focal depths in Hainaut (<6 km) are not completely out of the valid range of most GMPEs and that in our evaluation focal depth is taken into account for any GMPE having a depth term, divergence between models and data likely reflects a difference between modelled and actual crustal attenuation.

Another aspect concerns the magnitude range of Hainaut seismicity with respect to the range considered in PSHA. First, even though the magnitudes are rather low, the damaging character of these earthquakes in a densely populated area implies that they are relevant from an engineering point of view, and hence should be included in PSHA. This requires a

Table 1 – Parameters of earthquakes in the Hainaut area used in this study. Numbers in column 1 correspond to numbered epicentres in Fig. 1

Nr	ID	Date	Lon (°)	Lat (°)	Depth (km)	M_W	Num. IDPs (all / I ≥ 2)	Imax
1	449	1911-04-12	3.92	50.44	2.4	3.1	54 / 21	4.0
2	465	1911-06-01	4.46	50.45	4.3	3.9*	37 / 37	6.0
3	466	1911-06-03	4.45	50.46	1.4	4.0*	11 / 5	7.0
4	476	1920-01-17	3.82	50.44	1.6	3.5*	12 / 3	6.0
5	488	1931-05-09	4.15	50.466	0.6	3.0*	5 / 1	4.5
6	505	1936-11-05	4.3	50.47	2.2	3.3	5 / 5	4.5
7	517	1940-01-07	4.17	50.47	1.5	3.5	14 / 14	5.0
8	519	1940-01-09	4.17	50.48	2.8	3.3	5 / 5	4.5
9	534	1949-04-03	4.08	50.46	2.2	4.1*	94 / 70	7.0
10	538	1949-04-14	4.07	50.46	3.7	3.5	14 / 8	5.0
11	539	1949-04-14	4.06	50.46	2.4	3.6*	20 / 9	6.0
12	547	1952-10-21	3.88	50.43	2.9	3.1	66 / 18	4.0
13	548	1952-10-22	3.9	50.42	3.0	2.8	64 / 10	4.0
14	549	1952-10-27	3.87	50.43	3.5	3.5	69 / 39	5.0
15	562	1954-07-10	3.9	50.44	3.3	3.5	48 / 32	5.5
16	582	1965-12-15	4.12	50.45	2.7	4.0	108 / 46	7.0
17	587	1966-01-16	4.24	50.46	2.6	2.9*	133 / 21	4.5
18	588	1966-01-16	4.26	50.47	3.3	3.5	128 / 32	5.0
19	589	1966-01-16	4.26	50.46	2.1	4.0	132 / 57	7.0
20	597	1967-03-28	4.28	50.46	3.0	4.1	140 / 54	7.0
21	603	1968-08-12	4.21	50.46	2.3	3.6	25 / 25	5.0
22	606	1968-08-13	4.21	50.46	2.3	3.9	37 / 37	6.0
23	607	1968-09-23	4.23	50.46	2.8	3.2	35 / 22	5.0
24	608	1968-09-23	4.22	50.47	2.4	3.0	35 / 22	4.0
25	612	1970-11-03	4.41	50.41	2.3	3.6	39 / 26	5.0
26	627	1976-10-24	4.02	50.36	5.5	3.9*	59 / 36	5.0
27	641	1982-09-14	4.24	50.44	3.5	3.4*	33 / 16	4.0
28	651	1983-11-08	5.515	50.628	5.8	4.6	131 / 131	7.0

Moment magnitudes marked with * are based on empirical relationship with M_L established for the Hainaut area (Camelbeeck et al. 2022)

minimum magnitude not lower than $M_W = 4.0$, which more or less corresponds to the standard used in past national hazard maps. This value ensures that all earthquakes that caused maximum intensities of VII are included (Table 1). Second, the maximum magnitude hitherto considered in Hainaut was generally similar to that in other seismic zones in Belgium, a value which is significantly higher than the largest observed magnitude. The magnitude-frequency relation established from the observed magnitudes was simply extended to this maximum magnitude. However, if seismicity is indeed mining-related, much larger events would not be expected and a lower maximum magnitude would be more appropriate. It is thus recommendable to adjust both the minimum and maximum magnitudes in PSHA for this specific region.

On the other hand, we are also aware that the earthquake magnitudes in our dataset are close to or just below the lower limit of the valid magnitude range of most GMPEs and

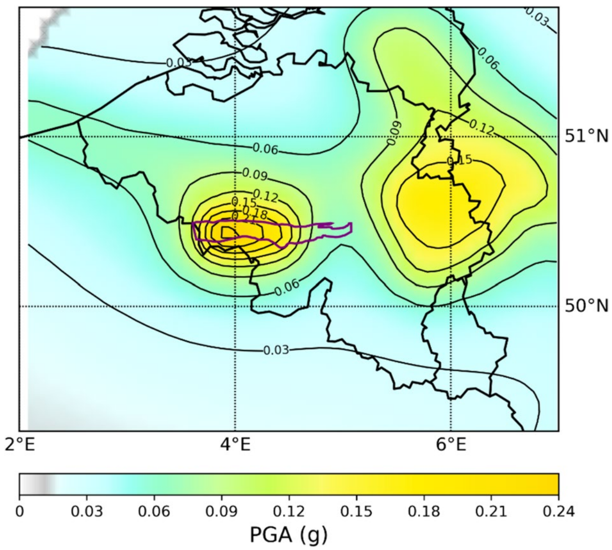

Fig. 4 Seismic hazard map (PGA, 10% probability of exceedance in 50 yr) for Belgium resulting from the SHARE project (Woessner et al. 2015). Purple polygon outlines Hainaut coal basin (but note that its shape is not exactly the same as the area source used to compute the hazard map)

the question may be raised if our results are representative of the magnitude range used in PSHA. Still, six earthquakes have $M_W \geq 4.0$, and if we allow for an uncertainty of 0.2 magnitude units, nine earthquakes have $M_W \geq 3.8$, representing ~ 59% of the available IDPs. We will therefore check the validity of our results by comparing them with those obtained with a subset of our intensity data related to the higher magnitudes.

Given the limited magnitude range of our dataset, it is clear that the selected GMPEs fitting best with the intensity data should not be indiscriminately applied to much larger magnitudes. This is not necessarily problematic for PSHA because, as argued above, if seismicity in Hainaut is indeed mining related, then it is also more sensible to consider a relatively low maximum magnitude in this area. Likewise, it is appropriate to use the best matching GMPEs for generating ShakeMaps of past and potential future events with comparable magnitudes in this area.

4 Methodology

4.1 Conversion between ground motion and macroseismic intensity

As most significant earthquakes in the Hainaut area occurred during the pre-digital era, instrumental ground-motion data are scarce. On the other hand, the macroseismic intensity data compiled by Camelbeeck et al. (2022) represent a wealth of data covering more locations at short distances than would be possible even with the current instrumental network. However, using such data to evaluate GMPEs requires an additional conversion step between predicted ground motions and intensities using a ground-motion-to-intensity conversion equation (GMICE).

Several GMICEs are available in literature. They are based on regression between the logarithm of instrumentally recorded ground motion, commonly peak ground acceleration (PGA) and/or peak ground velocity (PGV), and macroseismic intensity (MMI, MCS or mixed scale) at the same or nearby locations. We evaluated four relations:

AK2007 (Atkinson and Kaka 2007), FC2006 (Faccioli and Cauzzi 2006), FM2010 (Faenza and Michelini 2011), and GC2020 (Gomez-Capera et al. 2020). These relations differ in the intensity scale used, the shape of the regression (linear, bilinear or non-linear), the region where the data were collected, and the valid magnitude and intensity ranges, as indicated in Table 2.

Among these relations, AK2007 is the only one that contains optional magnitude and distance correction terms, derived from the residuals of the regression with intensity. Although it has been shown recently that the way this magnitude-distance dependency has been modelled introduces a bias for ground motions away from the median (Gallahue and Abrahamson 2023), our results should not be affected by this bias as we only convert median values. We first evaluated the effect of these correction terms on the residuals between observed intensities and median PGA and PGV values predicted by the GMPE of Akkar et al. (2014), converted to intensity with AK2007 and the other GMICEs. The results are shown in Fig. 5. Note that the main point here is not how well the GMPE fits the observations, as that depends on the GMPE used, but the consistency (or lack thereof) between the residuals obtained using PGA and PGV, and among the different GMICEs. The figure shows that applying the magnitude-distance correction term leads to a better agreement between the residuals based on PGA and PGV. This is mainly due to a shift in the residuals based on PGA, whereas the residuals based on PGV are less affected. For all other GMICEs, the results based on PGA and PGV differ significantly. Based on this finding, we selected the AK2007 relation with the magnitude-distance correction for comparing GMPEs with the Hainaut intensity data. However, our dataset only includes intensities evaluated using the EMS-98 macroseismic scale. In our analysis, we consider that these intensities would be similar if they were evaluated on the MMI scale used in AK2007, as it has been shown that these scales are approximately interchangeable (Musson et al. 2010). In agreement with the lower bound of the valid intensity range (Table 2) of most GMICEs, we discarded intensity values of 1 (not felt) in our dataset, decreasing the number of IDPs from 1553 to 802 (see Table 1). According to Wald et al. (1999), low intensity levels (MMI < VII) correlate fairly well with both PGA and PGV, but high intensities (MMI ≥ VII) correlate better with PGV. Considering that our dataset contains intensities up to VII, and that conversion from PGV to intensity using the selected GMICE (AK2007) is less affected by the magnitude-distance correction than conversion from PGA, we will attribute a higher weight to the GMPE ranking results based on PGV, although we will compute them for both intensity measures.

Table 2 Properties of the ground-motion-to-intensity conversion equations (GMICEs) evaluated in this study

GMICE	Region	Intensity scale	Regression shape	Mag. range	Intensity range
AK2007	Central US & California	MMI	Bilinear	2.5–7.4	2–9
FC2006	Italy	MCS/MSK	Linear	3.8–7.4	4.5/5–9
FM2010	Italy	MCS	Linear, bilinear (*)	3.0–6.9	2–8
GC2020	Italy	MCS	Exponential	4.2–6.8	2–10/11

MMI: Modified Mercalli Intensity, MCS: Mercalli-Cancani-Sieberg, MSK: Medvedev-Sponhauer-Karnik, (*) denotes regression shape used in this study

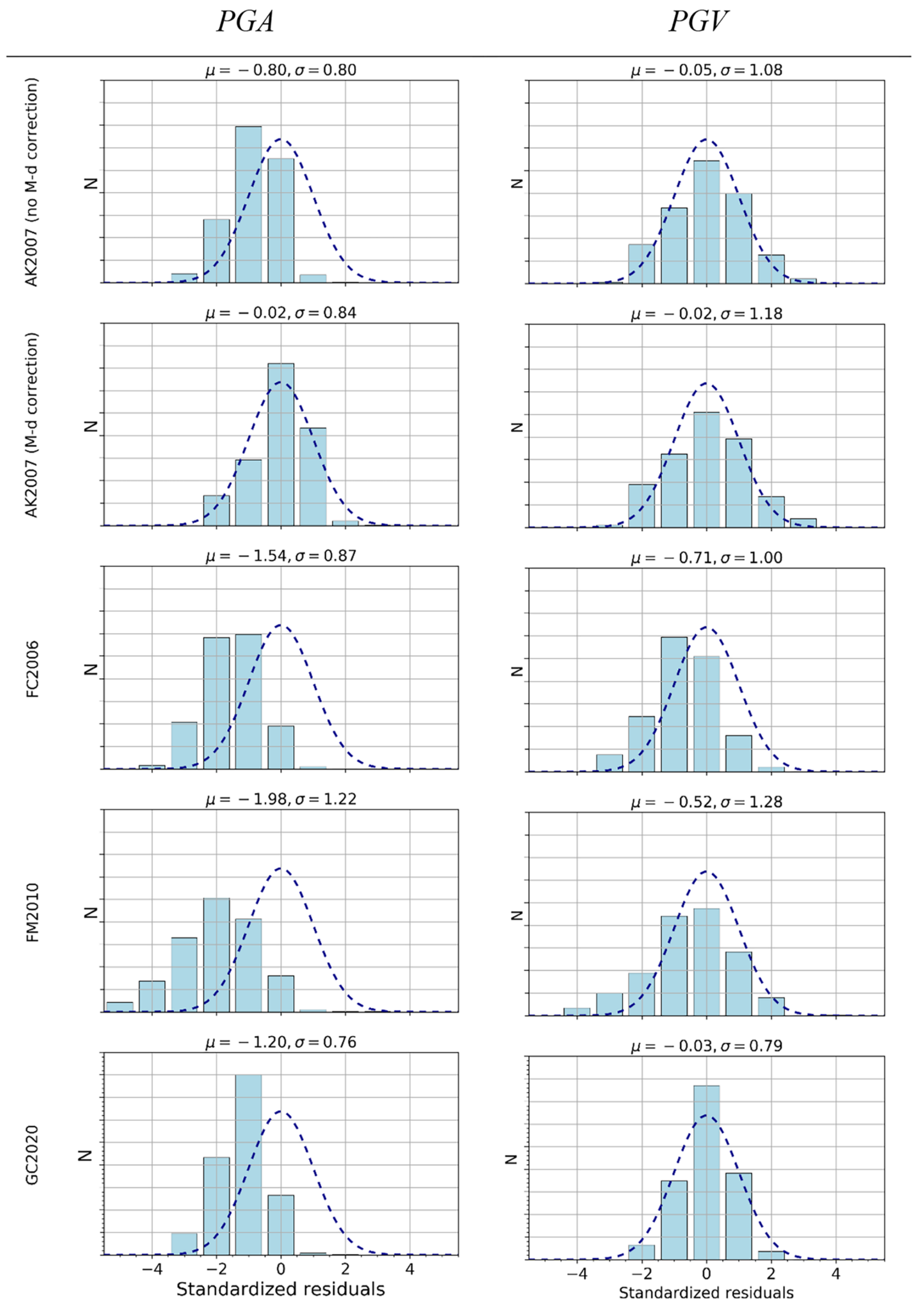

Fig. 5 Histograms of standardized residuals between observed intensities in the Hainaut area and peak ground motions (left column PGA, right column PGV) predicted by the Akkar et al. (2014) GMPE (with hypocentral distance metric), converted to intensities with different GMICEs (rows). Dashed line represents the standard normal distribution. Negative residuals correspond to overprediction, positive residuals to underprediction

4.2 GMPE testing

In the past two decades, several metrics have been proposed to evaluate the goodness of fit between a GMPE and observed ground motion. Scherbaum et al. (2004) proposed the LH (likelihood) measure, which is based on the absolute standardized residuals. It is intended to quantify the model fit, but also how well the underlying statistical assumptions are met: if both the mean and variance of the observed and predicted data match, LH is evenly distributed between 0 and 1. LH can be represented as a histogram but is often reduced to the median LH, with a value of 0.5 corresponding to a perfect match, whereas lower or higher values indicate that either the model is biased or that there is a difference between model variance and sample variance. Another measure, LLH (log-likelihood), based on information theory, was proposed by Scherbaum et al. (2009). It is calculated from the probabilities given by the GMPE to predict the observations. Similar to Villani et al. (2019), we compute LLH with the base-2 logarithm and change the sign of the results to obtain positive values. Again, the LLH is represented as a histogram, but this time with higher degrees of skewness towards lower values indicating a better match. Differences in average LLH between two models are a good estimate of the relative information loss and can be used to rank GMPEs, which is an advantage over the LH measure. However, LLH doesn't solve the issue that it is not possible to distinguish between model bias and different variance of model and observations. It has also been criticised (Kale and Akkar 2013) for focusing on models that can accurately represent the aleatory variability of the dataset, and hence for favouring GMPEs with large standard deviations. To remedy this, Kale and Akkar (2013) proposed the EDR (Euclidean-based distance ranking) measure, which is composed of three indexes: (1) MDE (modified Euclidean distance), which represents the total probability of the differences between the observed and predicted data over a range of sigma values, and generally lies between 0.5 and 3.2; (2) Kappa (κ), which measures the level of bias between the median predictions and the overall trend (with ground-motion amplitude) in the observed data, and the optimum value of which is 1.0; and (3) EDR, which is the overall ranking based on both the normalized MDE and $\sqrt{\kappa}$. MDE (and hence EDR) is hard to visualize, but we show the other measures in Fig. 6 for an ideal dataset obtained by random simulation of ground motions with the GMPE of Akkar et al. (2014) for a range of magnitudes, epicentral distances and focal depths. When GMPEs are compared to intensity data, standardized residuals between observed and predicted intensities are computed using the combined uncertainty of GMPE and GMICE (Villani et al. 2019). The subplots in Fig. 6 show histograms of standardized residuals (similar to Fig. 5) and of LH and LLH, as well as a plot of observed versus predicted ground motions and the fitted κ value. These provide a visual means to evaluate the goodness of fit according to these different measures.

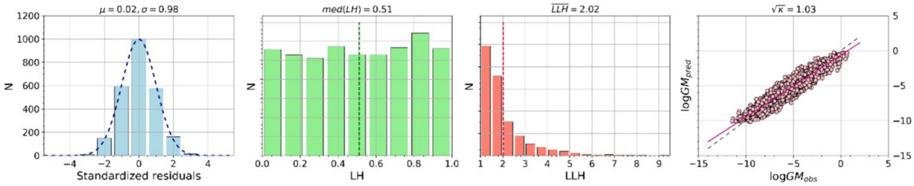

Fig. 6 Goodness-of-fit measures for an ideal dataset obtained by random simulation (2500 samples). From left to right: histogram of standardized residuals compared to the standard normal distribution; LH histogram (Scherbaum et al. 2004); LLH histogram (Scherbaum et al. 2009); $\sqrt{\kappa}$ (Kale and Akkar 2013). See text for an explanation of the LH, LLH and Kappa measures

5 GMPE selection

We selected more than 20 GMPEs for the analysis (Table 3). This selection contains updated versions of GMPEs applied in site-specific PSHA studies in Belgium during the past decade (Vanneste et al. 2014), GMPEs used in recent national PSHA studies in neighbouring countries like France (Drouet et al. 2020), Germany (Grünthal et al. 2018) and the United Kingdom (Mosca et al. 2022; Villani et al. 2019), as well as a number of additional GMPEs including some developed specifically for induced earthquakes. These GMPEs can be organized in different "families", depending on the underlying ground-motion dataset: Europe (n = 4), NGA-West (n = 6), NGA-East (n = 4), Global (n = 1), Japan (n = 2) and local GMPEs developed for specific countries or regions in NW Europe (n = 4). Among the induced-seismicity GMPEs (n = 5), Atkinson (2015) is based on a subset of NGA-West2, Bommer et al. (2019) was developed for induced earthquakes in the Groningen gas field in the Netherlands, Convertito et al. (2012) for induced seismicity in the Geysers geothermal field in California, McGarr and Fletcher (2005) for earthquakes induced by coal mining in Utah, and Douglas et al. (2013) for geothermally induced seismicity (although the authors note that ground motions from such events cannot be statistically distinguished from those of natural seismicity). The latter GMPE actually contains 36 different relations, corresponding to different combinations of stress drop (1, 10 and 100 bar), attenuation quality factor Q (200, 600 and 1800) and high-frequency kappa attenuation factor (0.005, 0.02, 0.04 and 0.06 s). The latter should not be confused with the Kappa score in EDR. In some national PSHA studies, host-to-target adjustments were applied to the selected GMPEs, but these were not considered here, except for the host-to-target adjustments of the NGA-East GMPEs of Campbell (2003) and Toro (2002). The latter were developed in the European SHARE project (Woessner et al. 2015) and applied in site-specific PSHA studies in Belgium. We applied the standard versions of these GMPEs as implemented in the open-source hazard engine OpenQuake (Pagani et al. 2014; https://github.com/gem/oq-engine). In several cases, different implementations are available, corresponding to different distance metrics (e.g., hypocentral or Joyner-Boore distance), assumed stress drop, whether style of faulting is taken into account, or which horizontal components are used. We tested all available implementations but show only the one giving the best result. For the Kotha et al. (2020) GMPE, we considered both the general form and an adapted form for application in the 2020 European Seismic Hazard Model (Weatherill et al. 2020). The latter contains calibrations for five main regions in Europe, but we only considered the default region 0, as Hainaut is not located in one of the main zones, and no regionalization is defined for PGV anyway. Two GMPEs are not implemented in OpenQuake: we obtained code for the Bommer et al. (2019) GMPE from the Royal Netherlands Meteorlogical Institute KNMI (Kruiver, pers. comm.), and we coded the McGarr and Fletcher (2005) GMPE ourselves. The former is based on local magnitude instead of moment magnitude; we used M_L values in this case as the M_L scale in Belgium is very similar to that in the Netherlands ($|\Delta M_L| = 0.1 \pm 0.2$) based on our comparison of both earthquake catalogues. As indicated in Table 3, some GMPEs are not defined for PGA or PGV, and some of these (mainly induced-seismicity GMPEs) are not defined for spectral acceleration either. These latter ones are only included for reference but are not eligible for selection as they cannot be used for state-of-the-art SHA. For GMPEs containing a site term, we always consider a value of 800 m/s for V_{S30} (average shear-wave velocity in the upper 30 m), which corresponds to standard rock site conditions. This is justified because in most of the Hainaut coal basin, either Cretaceous limestones (in the west) or Carboniferous mud- and sandstones (in the

Table 3 Overview of selected GMPEs, based on recent PSHA studies in Belgium and neighbouring countries, and organized in GMPE "families" (depending on underlying database)

	Belgium (Vanneste et al. 2014)	UK (Mosca et al. 2022; Villani et al. 2019)	Germany (Grünthal et al. 2018)	France (Drouet et al. 2020)	Other
Europe	Akkar et al. (2014) Bindi et al. (2014)	Akkar et al. (2014) Bindi et al. (2014)	Akkar et al. (2014) Bindi et al. (2014) Derras et al. (2014)		Kotha et al. (2020)
NGA-West	Boore and Atkinson (2008)	Boore et al. (2014) Chiou and Youngs (2014) Campbell and Bozorgnia (2014)	Bindi et al. (2017) *	Abrahamson et al. (2014)	
NGA-East	Atkinson and Boore (2006) Campbell (2003, SHARE) * Toro (2002, SHARE) *	Atkinson and Boore (2006)			Yenier and Atkinson (2015)
Japan (crustal)	Zhao et al. (2006) *				
Global	Cauzzi et al. (2015)	Cauzzi et al. (2015)	Cauzziet al. (2015)	Cauzzi et al. (2015)	
Local	Rietbrock et al. (2013)	Rietbrock et al. (2013) Rietbrock and Edwards (2019)		Ameri et al. (2017) * Drouet and Cotton (2015)	
Induced seismicity					Atkinson (2015) Bommer et al. (2019) °^ Convertito et al. (2012) *^ Douglas et al. (2013) McGarr & Fletcher (2005) ^

Legend: * Not defined for PGV, ° Not defined for PGA, ^Not defined for SA east) are at or near the surface (Fig. 1); only in the centre, there is a thin (< 20 m) deposit of Tertiary and Quaternary sediments.

6 GMPE testing results and ranking

For each tested GMPE, we compute predicted median ground-motion values (PGA or PGV) and corresponding uncertainties at the sites corresponding to the observed macroseismic IDPs. Earthquake ruptures are modelled as point sources (a valid approximation considering the moderate magnitudes) at the inferred hypocentres, and assuming a strike-slip mechanism. These ground-motion values and uncertainties are converted to macroseismic intensities and corresponding uncertainties using the selected GMICE. Finally, goodness-of-fit measures are computed with respect to the observations. The results can be visualized in plots similar to Fig. 6 for each GMPE separately, but to allow a better comparison of the performance of different GMPEs, we plot the five goodness-of-fit measures in spider diagrams, grouped by GMPE family. These are shown in Fig. 7 (PGV) and Fig. SI-1 in Online Resource 1 (PGA). Note that values in these plots are normalized such that scores improve outward from the centre of the plot; the real values can be found in Table SI-2 (PGV) and Table SI-3 (PGA) in Online Resource 1. For the DouglasEtAl-2013Stochastic GMPE, we only show the relation for a stress drop of 100 bar, Q-factor 200 and Kappa 0.02 s, which resulted in the best scores for both PGV and PGA. The scores for all forms of this GMPE are listed in Table SI-4 (PGV) and Table SI-5 (PGA) in Online Resource 1.

To rank the tested GMPEs, we consider EDR as the most important measure, followed by κ, and then the other measures. Based on our evaluation of GMICE performance, we also consider scores based on PGV more important than those based on PGA, but GMPEs performing well for both PGV and PGA are ranked higher. The selected European GMPEs perform quite similarly, with relatively good LH, LLH and MDE scores, but poor EDR and κ scores for PGV. PGA gives better results for LH, LLH and κ, but worse for MDE. Overall, the DerrasEtAl2014 GMPE performs best, but its κ score is not considered good enough for inclusion in our selection. The local GMPEs show large variations. We note the good κ score for the RietbrockEdwards2019Up GMPE for both PGV and PGA, but its other scores are too low. On the other hand, the DrouetAlpes2015Rrup GMPE scores relatively well, except for κ, and the scores also deteriorate for PGA. The NGA-West GMPEs perform very similarly to the European GMPEs for PGV, i.e. acceptable LH, LLH and MDE scores, but poor κ and EDR scores. For PGA, all scores go down, except those of the BooreAtkinson2008Prime GMPE, but its κ score is not good enough. Among the NGA-East GMPEs, the AtkinsonBoore2006Modified2011 GMPE performs best: for PGV, it shows good LH, LLH and MDE scores and moderate κ and EDR scores, which further improve for PGA. We consider this an acceptable GMPE for selection. The only global GMPE that we tested shows acceptable LH, LLH and MDE scores, but very poor κ and EDR scores for PGV; most scores improve only slightly for PGA. The Japanese GMPEs can only be evaluated based on PGA, but their κ and EDR scores are too poor. Finally, the induced-seismicity GMPEs yield clearly better scores than the other GMPE families. For PGV, both the Atkinson2015 and DouglasEtAl2013Stochastic GMPEs show overall good scores, including κ and EDR; for PGA, these scores even improve along with LLH. Although their MDE score goes slightly down for PGA, as well as the LH score for the DouglasEtAl2013Stochastic GMPE, both GMPEs are selected. The BommerEtAl2019_GM and

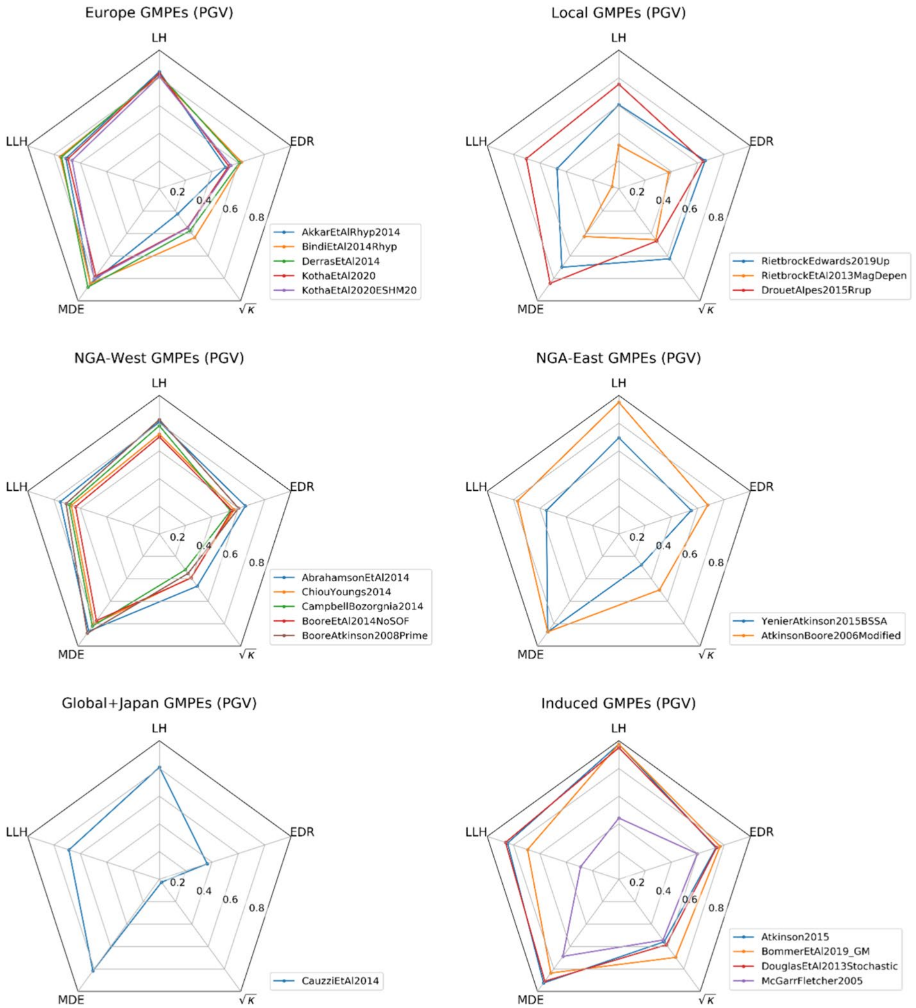

Fig. 7 Spider diagrams showing goodness-of-fit measures for PGV predicted by different GMPEs converted to intensity with the AK2007 GMICE with respect to the Hainaut intensity data. GMPEs are grouped by "family" (see Table 3). DouglasEtAl2013Stochastic GMPE corresponds to stress drop of 100 bar, Q-factor 200 and Kappa 0.02 s. Goodness-of-fit measures are normalized to different minimum and maximum values (LH: |med(LH) − 0.5| * 2; $\overline{\text{LLH}}$: 1.75–3.75; MDE: 1–2; $\sqrt{\kappa}$: 1–2.5; EDR: 1–4)

ConvertitoEtAl2012Geysers GMPEs also perform very well for PGV and PGA, respectively, but were not selected as they are not defined for spectral acceleration.

Our results indicate that the induced-seismicity GMPEs, in particular the GMPEs of Atkinson (2015) and Douglas et al. (2013), along with the NGA-East GMPE by Atkinson and Boore (2006), show the overall best fit with the Hainaut intensity data. Their scores for both PGV and PGA are shown separately in Fig. 8 (top row), while plots of different goodness-of-fit measures are shown in Fig. 9. The latter can be compared to the goodness-of-fit plot for a GMPE with a particularly bad fit in Fig. 10. We consider these three GMPEs as the most appropriate ones for seismic hazard assessment in the Hainaut seismic zone. To

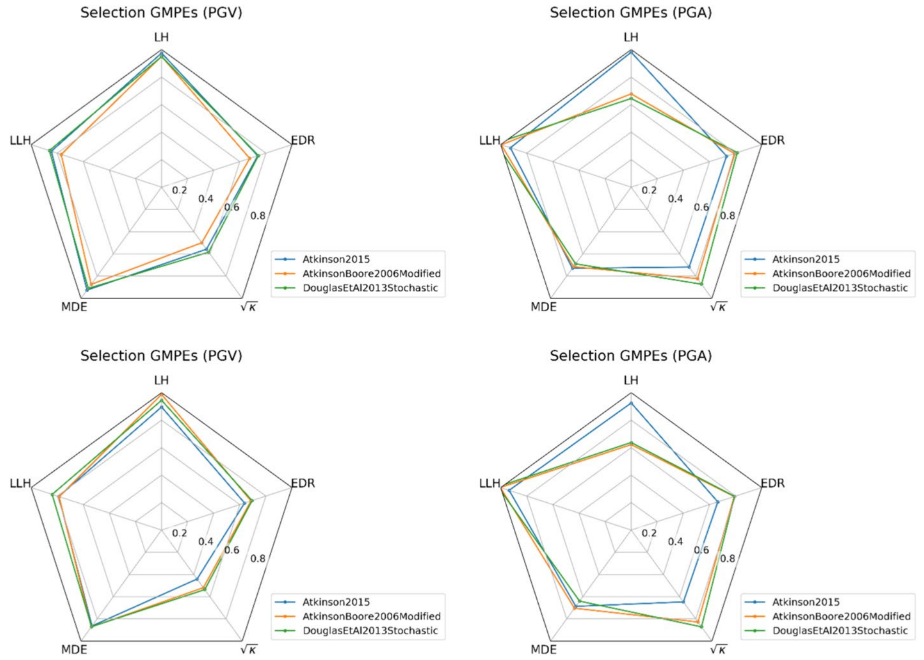

Fig. 8 Same as Fig. 7, but for GMPEs with best goodness-of-fit. Left: based on PGV; Right: based on PGA; Top: using all IDPs (n = 802); Bottom: using only IDPs from earthquakes with $M_W \geq 3.8$ (n = 473)

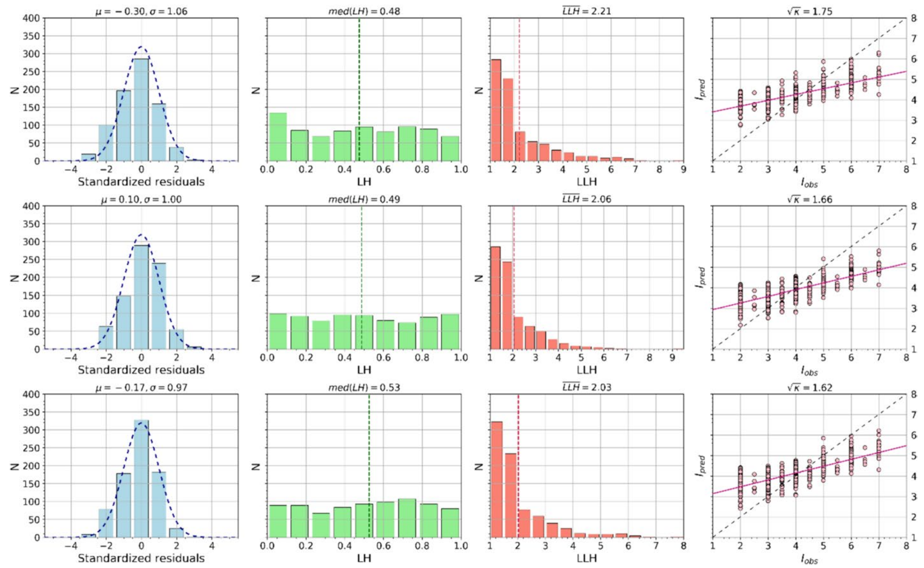

Fig. 9 Goodness-of-fit measures for PGV predicted by final selection of GMPEs converted to intensity with the AK2007 GMICE with respect to Hainaut intensity data. Top: AtkinsonBoore2006Modified2011 GMPE; Middle: Atkinson2015 GMPE; Bottom: DouglasEtAl2013StochasticSD100Q200K020 GMPE. See Fig. 6 for explanation of subplots

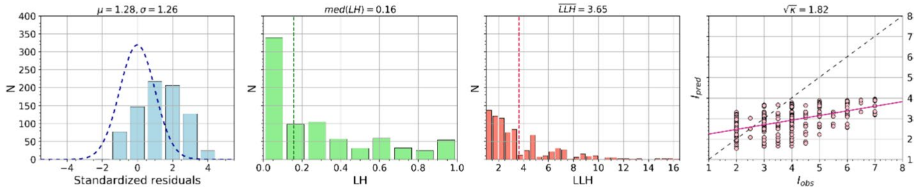

Fig. 10 Goodness-of-fit measures for PGV predicted by RietbrockEtAl2013MagDependent GMPE with respect to Hainaut intensity data. See Fig. 6 for explanation of subplots

verify whether our results are biased by earthquake magnitudes that are too far below the validity range of the tested GMPEs, we also calculated the scores for the selected GMPEs using a subset of 473 IDPs associated with earthquakes with $M_W \geq 3.8$. These scores are shown in Fig. 8 (bottom row). The differences with the full dataset are relatively small, which validates our approach. However, it should be noted that none of the tested GMPEs provides a good match. Compared to Villani et al. (2019), who did a similar study using macroseismic data from the United Kingdom, our best-matching GMPEs yield LLH and MDE values that are comparable or even slightly better, but the κ and EDR scores are significantly worse than their best scores ($\sqrt{\kappa}$: 1.06–1.21, EDR: 1.26–1.27; compare with Tables SI-2 to SI-5 in Online Resource 1). Similarly, we can compare with the goodness of fit calculated for the intensity prediction equation (IPE) fitted to the Hainaut intensity data by Camelbeeck et al. (2022). The plot in Fig. 11 clearly shows a κ score that is much better than that of any GMPE we tested.

Furthermore, we note that none of the ranking methods considers the trend of residuals with distance, i.e. the attenuation term of the GMPE. As the κ score measures the trend with increasing observed ground motion, and ground motion generally decreases with distance, this score could be considered as a proxy for the distance trend, but it does not indicate whether this trend is positive or negative. We evaluate the distance trend more explicitly in Fig. 12 for three models: one of the three best-matching GMPEs (Atkinson215), a poorly fitting GMPE (RietbrockEtAl2013MagDependent) and the region-specific IPE (CamelbeeckEtAl2022Hainaut). Each subplot shows the residuals rounded to 0.5 degrees (similar to the resolution of the observations) versus epicentral distance. We compute the average distance trend (thick magenta line) as the weighted average of the trends of the individual earthquakes (thin lines in different colours). The weights correspond to the product of the distance covered by the observations (97.5th percentile) and the number of observations divided by 10, and we require at least 10 observations to contribute. An upward/downward trend indicates that the evaluated

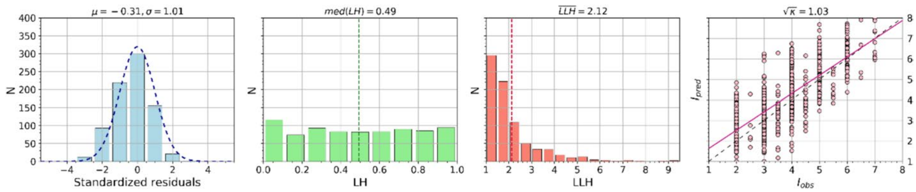

Fig. 11 Goodness-of-fit measures for the IPE of Camelbeeck et al. (2022) for the Hainaut region. See Fig. 6 for explanation of subplots

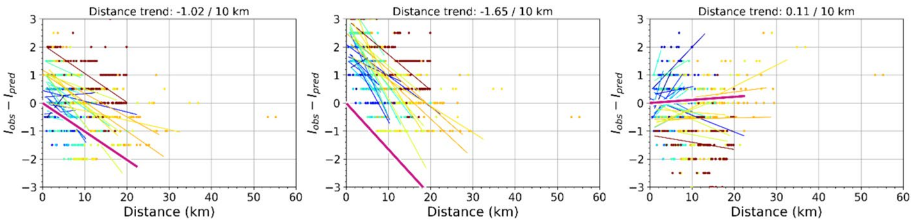

Fig. 12 Distance trends of residuals for different models. Note that residuals have been rounded to the nearest half degree. Magenta line corresponds to the average distance trend, other coloured lines indicate the distance trend for individual earthquakes. Left: Atkinson2015 GMPE, Middle: RietbrockEtAl2013MagDependent GMPE; Right: CamelbeeckEtAl2022Hainaut IPE

GMPE attenuates faster/slower than the observed intensities. The average distance trends of all models are reported (as intensity degrees per 10 km) in Tables SI-2 to SI-5 in Online Resource 1. All tested GMPEs yield negative (downward) distance trends. For the modelling based on PGV, most GMPEs show distance trends between − 1.15 and ~ − 1.5; only the three selected GMPEs which scored best in the other categories, along with some non-eligible induced-seismicity GMPEs have distance trends close to -1. This is in good agreement with our earlier observation that intensities generated by earthquakes in the Hainaut area generally attenuate 3 degrees faster over a distance of 30 km than elsewhere in Belgium. The distance trends based on PGA are significantly better for most GMPEs, but the selected GMPEs still score among the best (between − 0.39 and − 0.67), so there is no reason to adjust our selection.

The differences in distance trend can also be evaluated by directly comparing observed and predicted intensities as a function of distance for a particular earthquake. We selected the $M_W = 4.1$ 1949 earthquake for this purpose, as it has the largest number of IDPs in the Hainaut region (see Table 1). The results are shown in Fig. 13, again for three model sets: the three best-matching GMPEs, a GMPE with a particularly bad fit, and the region-specific IPE. It can be seen that the best-matching GMPEs attenuate fast at short epicentral distances, but their attenuation curves flatten significantly beyond 10 km distance, in contrast to the region-specific IPE. The limitation of the fit to short epicentral distances also explains why a GMPE (AtkinsonBoore2006Modified2011) of the NGA-East family, which is generally characterized by slow attenuation, may still show a relatively good distance trend with respect to the Hainaut intensity data.

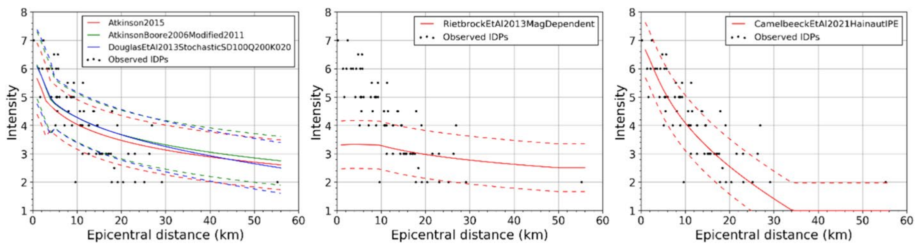

Fig. 13 Comparison of observed and predicted intensities (converted from PGV to intensity with the AK2007 GMICE for GMPE models) as a function of epicentral distance for the $M_W = 4.1$ 1949 earthquake (ID 534 in Table 1). Left: selected GMPEs; Middle: RietbrockEtAl2013MagDependent GMPE; Right: CamelbeeckEtAl2022 IPE

The limited goodness-of-fit with mainly induced-seismicity GMPEs is in agreement with the specific characteristics of seismicity in the Hainaut region. This is also the case for the version of the DouglasEtAl2013Stochastic GMPE showing the best fit: relatively high stress drop (100 bar), low Q-factor (200) and intermediate kappa-factor (0.02 s), which is in agreement with the idea that seismicity in the Hainaut region is likely induced (and may thus be characterized by rather high stress drops) and with higher attenuation than in other stable crustal areas of NW Europe. However, this does not necessarily prove that the Hainaut seismicity is induced. GMPEs for induced seismicity are evidently better tuned to the magnitude range (M 3–5) and shallow focal depth of seismicity in the Hainaut region, as well as to the distance range (few tens of km) of our intensity dataset.

7 Impact on seismic hazard

In all PSHA studies currently conducted in Belgium, the particular seismic activity in the Hainaut area is attributed to a dedicated source zone, which results in a relatively high hazard in this area and around it. The strong observed attenuation of intensities in the Hainaut area, as well as our comparison between intensity data and predicted ground motions, indicate the necessity to apply specific GMPEs for earthquakes in this area that better represent the attenuation there. To evaluate the influence of more appropriate GMPEs on seismic hazard in SW Belgium and northern France, we compare hazard maps based on our classical selection of GMPEs for stable shallow crust (SSC) in most of the Belgian territory (with the exception of the more active Roer Valley Rift System), with hazard maps where we apply the three best-matching GMPEs resulting from our analysis in the source zone corresponding to the Hainaut area. In both cases, the same source model and activity rates in each source are used.

Our current PSHA model, which was developed to evaluate hazard for critical facilities in Belgium in the past decade (Vanneste et al. 2014), consists of a source-model logic tree and a ground-motion logic tree. The source-model logic tree contains three different source models (Fig. 14): (1) the Leynaud_extended model, which corresponds to the original model of Leynaud et al. (2000) used for the current Belgian national annex to Eurocode 8 (Bureau de Normalisation (NBN), 2011), extended with area sources from the SHARE project (Woessner et al. 2015) to cover the entire Belgian territory; (2) the Seismotectonic model (Verbeeck et al. 2009) is a revision of the Leynaud model in which the limits between sources have been drawn in more detail and more closely following known geological structures and geophysical contrasts; (3) the TwoZonev2 model is a minimalistic model containing only two sources, the Roer Valley Rift System (RVRS) where seismic activity can be linked to active faults and the "Single Large Zone" (SLZ) closely bounding most seismicity outside the RVRS. In the former two models, the Hainaut area is represented by a separate zone ("Hainaut" in the Leynaud_extended model; "Mons-Orchies Basin" in the Seismotectonic model), whereas in the latter model it is part of the much larger SLZ. Weights of 0.285, 0.330 and 0.385 are attributed to these three source models, respectively. These weights are a combination of expert solicitation and weights reflecting the robustness with which magnitude-frequency distributions (MFDs) can be computed for individual sources. Further in the source-model logic tree, we consider 25 MFDs for each source reflecting the uncertainty on the Gutenberg-Richter b-value, in combination with 5 Mmax values, obtained for each tectonic region type following the EPRI approach (Cornell 1994; EPRI et al. 2012). The minimum magnitude was set to $M_W = 4.0$.

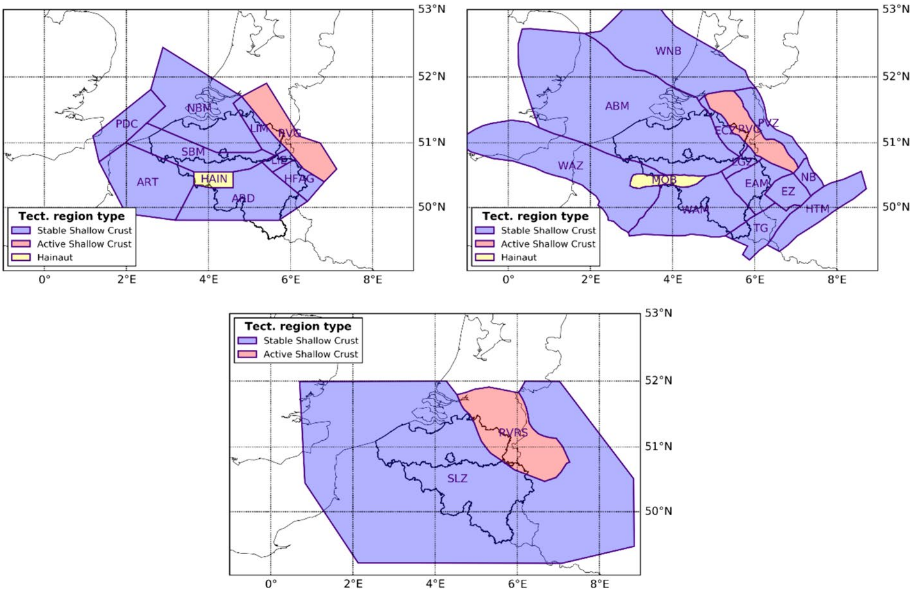

Fig. 14 Source models considered in PSHA computations. Top left: Leynaud_extended model; Top right: Seismotectonic model; Bottom: TwoZonev2 model. Colours correspond to tectonic region type, which is linked to the selection of GMPEs applied in each source

In the ground-motion logic tree, we consider different GMPE selections for the two tectonic region types (stable shallow crust and active shallow crust) in our source models. The classical selection for standard-rock conditions in PSHA studies in Belgium is listed in Table 4. The weights were derived from a semi-objective procedure to evaluate the suitability of each GMPE for application in Belgium. In this study, we compute hazard maps for different scenarios for the Hainaut area, one in which we apply the same GMPEs as in the other SSC sources (corresponding to current practice), and one in which we apply the three best-matching GMPEs based on our analysis (i.e., AtkinsonBoore2006Modified2011, Atkinson2015 and DouglasEtAl2013StochasticSD100Q200K020) with equal weights. This will allow evaluating the effect of a GMPE selection that is better adapted to the attenuation characteristics of the Hainaut region. In addition, we also consider a third scenario that takes into account the specific magnitude and depth range of Hainaut seismicity, which

Table 4 Classical selection of GMPEs for standard rock conditions and associated weights used in Belgian PSHA studies

Stable Shallow Crust (SSC)		Active Shallow Crust (ASC)	
GMPE	Weight	GMPE	Weight
AtkinsonBoore2006Modified2011	0.168	AkkarEtAl2013	0.288
AkkarEtAl2013	0.308	BindiEtAl2011	0.108
Campbell2003SHARE	0.288	BooreAtkinson2008Prime	0.288
FaccioliEtAl2010	0.168	FaccioliEtAl2010	0.188
ToroEtAl2002SHARE	0.068	ZhaoEtAl2006Asc	0.128

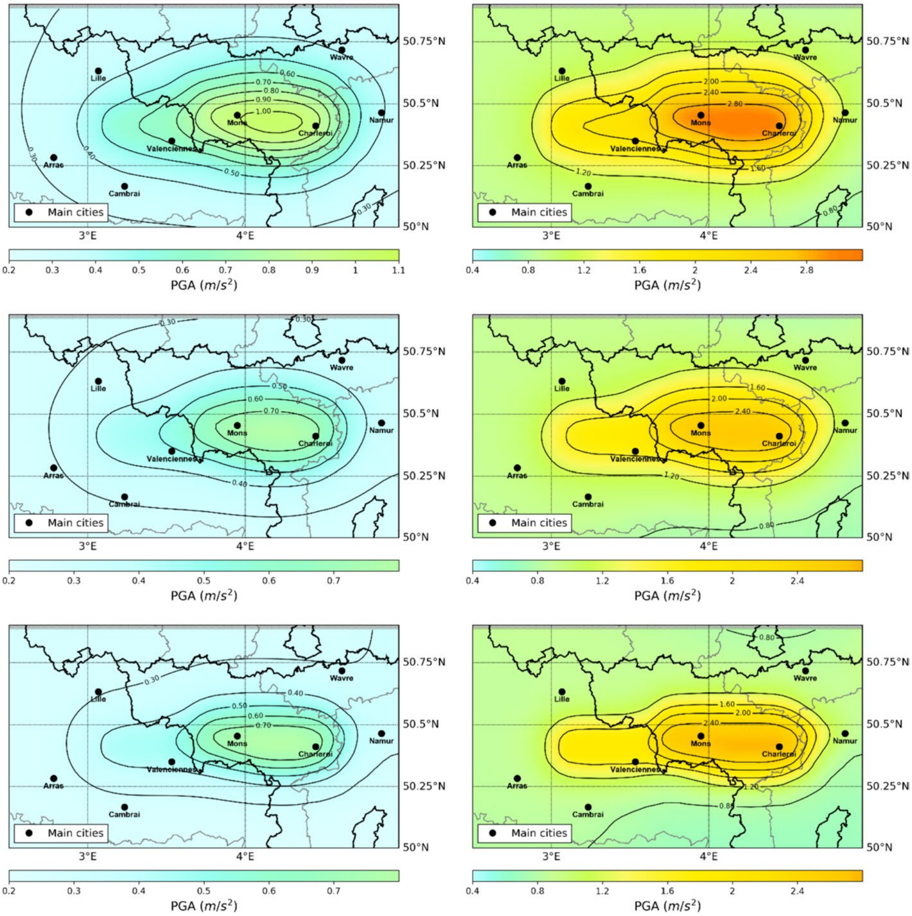

Fig. 15 Comparison of probabilistic seismic hazard maps for PGA in SW Belgium and northern France computed using different GMPE selections for the Hainaut area. Top: GMPEs for stable continental regions similar to the remainder of the Belgian territory (except for the RVRS); Middle: best-matching GMPEs from this study; Bottom: best-matching GMPEs in combination with adapted depth range and maximum magnitude for the area source corresponding to the Hainaut region. Left: 475-yr return period; Right: 3000-yr return period

also constrained the GMPE ranking. Different ways can be envisaged to do this. Here, we split the Hainaut area source into a shallow and a deep part, with the boundary at a depth of 7.5 km. In the shallow part, the best-fitting GMPEs are applied and the maximum magnitude is fixed to the highest observed magnitude plus 1 magnitude unit (i.e., $M_W = 5.1$), reflecting the possible mining-related nature of Hainaut seismicity. In the deep part, the GMPE selection and maximum magnitude are the same as in other SSC area sources. We thus assume that all deeper earthquakes are natural, the main example being the 1995 $M_L = 4.5$ Le Roeulx earthquake (see Fig. 1), which occurred close to the northern limit of the Hainaut coal basin at a depth of ~24 km. However, as it is not possible to compute the MFD for the deep part, the MFDs of adjacent area sources are redistributed according to their relative volumes.

We ran the computations with our custom software built on top of the core python module of OpenQuake (Pagani et al. 2014; https://github.com/gem/oq-engine). The results are demonstrated with hazard maps for PGA and for two return periods: 475 years (standard return period for normal buildings) and 3000 years (return period more suitable for more critical, non-nuclear, infrastructure). These maps are shown in Fig. 15. It should be noted that they are only intended as a proof of concept; they should not be considered as a final product and certainly do not replace the current hazard map. Simply using more appropriate GMPEs for the Hainaut area without other adjustments (middle panel in Fig. 15) results in a reduction of local seismic hazard compared to the classical GMPE selection (top panel in Fig. 15): 0.7 m/s^2 versus 0.9–1.0 m/s^2 for the 475-yr return period, and 2.4 m/s^2 versus 2.8 m/s^2 for the 3000-yr return period in the region between the cities of Mons and Charleroi. The impact seems to be more pronounced for short return periods, and relatively more important in the central Hainaut area compared to the region just outside. If we also consider a more appropriate magnitude and depth range for the Hainaut source zone (lower panel in Fig. 15), hazard levels do not necessarily decrease further inside the Hainaut region. The effects of a lower maximum magnitude and concentration of the seismic activity in a shallow source zone appear to counterbalance each other. However, the hazard contours are clearly tighter around the Hainaut region, resulting in lower hazard in the region just outside. We also found that this third scenario is very sensitive to the maximum magnitude considered in the shallow Hainaut source. A further reduction of hazard levels may be obtained if this parameter is revised downward. It is of course difficult to evaluate the reliability of these hazard maps, but the overall lower hazard levels and the tighter concentration of the highest levels around the Hainaut region are in better agreement with the maximum intensity maps (Fig. 3). Further adaptations may be considered to take into account the possible mining-related nature of the Hainaut seismicity, such as a different temporal occurrence model, but this is outside the scope of this study.

8 Conclusions

Seismicity in the Hainaut area in SW Belgium displays unusual characteristics compared to other regions in NW Europe: in less than a century the region was hit by a series of moderate-magnitude (M_W 2.8–4.1) earthquakes with shallow focus (<6 km) which were strongly felt and some of which caused local damage, resulting in a rich macroseismic dataset. However, there are no known earthquakes before the nineteenth century and seismicity has decreased significantly since the end of the twentieth century. This may point to a relation with coal mining in the region, as has been suggested before, but not yet convincingly demonstrated. If this is correct, this seismicity may be a transient phenomenon, as mining activities have come to a halt. At the very least, seismic hazard in the larger Hainaut region seems to be overestimated without specific adjustments. In addition, intensities in the Hainaut area appear to attenuate faster with distance than elsewhere in Belgium, which suggests that the classical GMPEs used in SHA do not adequately represent the specific character of seismicity in this area. In this study, we evaluated the goodness of fit of a wide range of GMPEs with respect to the available macroseismic intensity data through an intermediary conversion with a GMICE. We also defined an additional measure to characterize the residual trend with distance, which is lacking in literature. Our analysis indicates that (1) the GMICE of Atkinson and Kaka (2007) with magnitude-distance corrections yields the most consistent results for PGA and PGV; (2) None of the selected GMPEs show a good match with respect to the intensity dataset. In particular, the κ scores (Kale and Akkar 2013) are quite poor, and all GMPEs attenuate significantly slower with distance compared to the observed intensities; (3) two GMPEs for induced seismicity (Atkinson 2015; Douglas et al. 2013), along with the NGA-East GMPE of Atkinson and Boore (2006) show the best overall fit, although the fit is still far from perfect.

Given the limited magnitude and depth range of the dataset used to rank the GMPEs, the selection of best-fitting GMPEs should not be applied indiscriminately in PSHA. It is thus recommended to constrain the depth and maximum magnitude of the area source corresponding to the Hainaut region, which also reflects the possible mining-related nature of this seismicity. We also recommend setting the minimum magnitude not lower than 4.0 when calculating hazard for normal constructions, in accordance with the damaging character of these earthquakes. Seismic hazard maps computed with a mix of the best-fitting GMPEs show a reduction in hazard levels in the area by 20–30% compared to the selection of GMPEs that we use for stable shallow crust elsewhere in Belgium. If furthermore constrain seismic activity in Hainaut to a shallow source zone with a lower maximum magnitude, the overall hazard levels remain similar, but the highest hazard levels are more tightly focused inside the Hainaut region. We intend to repeat the ranking of GMPEs with macroseismic data for the remainder of the Belgian territory. Our results will be useful to guide the GMPE selection for the new seismic hazard map of Belgium as well as for generating ShakeMaps for future earthquakes in the Hainaut area. Our study is also of more general interest to regions where it is difficult to evaluate ground-motion models for use in SHA, but where earthquakes have occurred before the deployment of local seismic networks and only macroseismic intensity data are available.

Supplementary Information The online version contains supplementary material available at https://doi.org/10.1007/s10518-024-01958-1.

Acknowledgements We thank John Douglas and an anonymous reviewer for providing constructive comments that allowed us to improve our manuscript.

Author contribution KV: conceptualization, methodology, formal analysis, software, validation, visualization, original draft preparation, review and editing; BN: data curation, validation, visualization, review and editing; TC: conceptualization, data curation, methodology, validation, visualization, original draft preparation, review and editing.

Funding This study was financed with internal funds of the Royal Observatory of Belgium. The code to evaluate the goodness of fit of ground-motion models with respect to observed intensity data was developed in the frame of the BRAIN-be BELSHAKE project (Contract nr. B2/202/P1/BELSHAKE), funded by the Belgian Science Policy Office.

Data availability All macroseismic data points are publicly accessible as CSV-files for each earthquake on Zenodo (https://doi.org/10.5281/zenodo.10047233).

Declarations

Competing interests The authors declare that they have no conflict of interests.

References

Abrahamson NA, Silva WJ, Kamai R (2014) Summary of the ASK14 ground motion relation for active crustal regions. Earthq Spectra 30:1025–1055. https://doi.org/10.1193/070913EQS198M

Akkar S, Sandıkkaya MA, Bommer JJ (2014) Empirical ground-motion models for point- and extended-source crustal earthquake scenarios in Europe and the Middle East. Bull Earthq Eng 12:359–387. https://doi.org/10.1007/s10518-013-9461-4

Alexandre P, Kusman D, Petermans T, Camelbeeck T (2008) The 18 September 1692 Earthquake in the Belgian Ardenne and Its Aftershocks. In: Fréchet J, Meghraoui M, Stucchi M (eds) Historical seismology: interdisciplinary studies of past and recent earthquakes. Springer, Berlin, pp 209–230

Ameri G, Drouet S, Traversa P, Bindi D, Cotton F (2017) Toward an empirical ground motion prediction equation for France: accounting for regional differences in the source stress parameter. Bull Earthq Eng 15:4681–4717. https://doi.org/10.1007/s10518-017-0171-1

Atkinson GM (2015) Ground-motion prediction equation for small-to-moderate events at short hypocentral distances, with application to induced-seismicity hazards. Bull Seismol Soc Am 105:981–992. https://doi.org/10.1785/0120140142

Atkinson GM, Boore DM (2006) Earthquake ground-motion prediction equations for eastern North America. Bull Seismol Soc Am 96:2181–2205. https://doi.org/10.1785/0120050245

Atkinson GM, Kaka SLI (2007) Relationships between felt intensity and instrumental ground motion in the Central United States and California. Bull Seismol Soc Am 97:497–510. https://doi.org/10.1785/0120060154

Bindi D, Massa M, Luzi L, Ameri G, Pacor F, Puglia R, Augliera P (2014) Pan-European ground-motion prediction equations for the average horizontal component of PGA, PGV, and 5%-damped PSA at spectral periods up to 3.0 s using the RESORCE dataset. Bull Earthq Eng 12:391–430. https://doi.org/10.1007/s10518-013-9525-5

Bindi D, Cotton F, Kotha SR, Bosse C, Stromeyer D, Grünthal G (2017) Application-driven ground motion prediction equation for seismic hazard assessments in non-cratonic moderate-seismicity areas. J Seismolog 21:1201–1218. https://doi.org/10.1007/s10950-017-9661-5

Bommer JJ, Stafford PJ, Ntinalexis M (2019) Updated empirical GMPEs for PGV from groningen earthquakes – march 2019. NAM.

Boore DM, Atkinson GM (2008) Ground-motion prediction equations for the average horizontal component of PGA, PGV, and 5%-damped PSA at spectral periods between 0.01 s and 10.0 s. Earthq Spectra 24:99–138. https://doi.org/10.1193/1.2830434

Boore DM, Stewart JP, Seyhan E, Atkinson GM (2014) NGA-West2 equations for predicting PGA, PGV, and 5% damped PSA for shallow crustal earthquakes. Earthq Spectra 30:1057–1085. https://doi.org/10.1193/070113EQS184M

Bureau de Normalisation (NBN) (2011) Eurocode 8 - Calcul des structures pour leur résistance aux séismes - Partie 1: Règles générales, actions sismiques et règles pour les bâtiments - Annexe nationale.

Camelbeeck T (1985) Some notes concerning the seismicity in Belgium. Magnitude scale. Detection capability of the Belgian seismic stations. In: Melchior P (ed) Seismic activity in Western Europe, with particular consideration to the liege earthquake of november 8, 1983. Reidel, Dordrecht, pp 99–108

Camelbeeck T, Van Noten K, Lecocq T, Hendrickx M (2022) The damaging character of shallow 20th century earthquakes in the Hainaut coal area (Belgium). Solid Earth 13:469–495. https://doi.org/10.5194/se-13-469-2022

Campbell KW (2003) Prediction of strong ground motion using the hybrid empirical method and its use in the development of ground-motion (attenuation) relations in Eastern North America. Bull Seismol Soc Am 93:1012–1033

Campbell KW, Bozorgnia Y (2014) NGA-West2 ground motion model for the average horizontal components of PGA, PGV, and 5% damped linear acceleration response spectra. Earthq Spectra 30:1087–1114. https://doi.org/10.1193/062913EQS175M

Cauzzi C, Faccioli E, Vanini M, Bianchini A (2015) Updated predictive equations for broadband (0.01–10 s) horizontal response spectra and peak ground motions, based on a global dataset of digital acceleration records. Bull Earthq Eng 13:1587–1612. https://doi.org/10.1007/s10518-014-9685-y

Chiou BSJ, Youngs RR (2014) Update of the Chiou and Youngs NGA model for the average horizontal component of peak ground motion and response spectra. Earthq Spectra 30:1117–1153. https://doi.org/10.1193/072813EQS219M

Convertito V, Maercklin N, Sharma N, Zollo A (2012) From induced seismicity to direct time-dependent seismic hazard. Bull Seismol Soc Am 102:2563–2573. https://doi.org/10.1785/0120120036

Cornell CA (1994) Statistical analysis of maximum magnitudes. In: Johnston AC, Coppersmith KJ, Kanter LR, Cornell CA (Eds) The earthquakes of stable continental regions, Volume 1: assessment of large earthquake potential. Electric Power Research Institute (EPRI), pp. 5-1–5-27.

Derras B, Bard PY, Cotton F (2014) Towards fully data driven ground-motion prediction models for Europe. Bull Earthq Eng 12:495–516. https://doi.org/10.1007/s10518-013-9481-0

Descamps L (2009) Relations entre l'activité sismique dans le Hainaut et l'activité minière (M.Sc. thesis). University of Mons.

Douglas J, Edwards B, Convertito V, Sharma N, Tramelli A, Kraaijpoel D, Cabrera BM, Maercklin N, Troise C (2013) Predicting ground motion from induced earthquakes in geothermal areas. Bull Seismol Soc Am 103:1875–1897. https://doi.org/10.1785/0120120197

Drouet S, Cotton F (2015) Regional stochastic GMPEs in low-seismicity areas: scaling and aleatory variability analysis—application to the French Alps. Bull Seismol Soc Am 105:1883–1902. https://doi.org/10.1785/0120140240

Drouet S, Ameri G, Le Dortz K, Secanell R, Senfaute G (2020) A probabilistic seismic hazard map for the metropolitan France. Bull Earthq Eng 18:1865–1898. https://doi.org/10.1007/s10518-020-00790-7

EPRI, U.S. DOE, U.S. NRC (2012) Central and Eastern United States seismic source characterization for nuclear facilities. Palo Alto, California.

Faccioli E, Cauzzi C (2006) Macroseismic intensities for seismic scenarios estimated from instrumentally based correlations. In: Proceedings of the First European Conference on Earthquake Engineering and Seismology, pp 3–8

Faenza L, Michelini A (2011) Regression analysis of MCS intensity and ground motion spectral accelerations (SAs) in Italy. Geophys J Int 186:1415–1430. https://doi.org/10.1111/j.1365-246X.2011.05125.x

Gallahue M, Abrahamson N (2023) New methodology for unbiased ground-motion intensity conversion equations. Bull Seismol Soc Am 113:1133–1151. https://doi.org/10.1785/0120220224

Gomez-Capera AA, D'Amico M, Lanzano G, Locati M, Santulin M (2020) Relationships between ground motion parameters and macroseismic intensity for Italy. Bull Earthq Eng 18:5143–5164. https://doi.org/10.1007/s10518-020-00905-0

Grünthal G, Musson RMW, Schwarz J, Stucchi M (1998) European Macroseismic Scale 1998. Cahiers du Centre Européen de Géodynamique et de Séismologie

Grünthal G, Stromeyer D, Bosse C, Cotton F, Bindi D (2018) The probabilistic seismic hazard assessment of Germany—version 2016, considering the range of epistemic uncertainties and aleatory variability. Bull Earthq Eng 16:4339–4395. https://doi.org/10.1007/s10518-018-0315-y

Kale Ö, Akkar S (2013) A new procedure for selecting and ranking ground-motion prediction equations (GMPEs): the Euclidean distance-based ranking (EDR) method. Bull Seismol Soc Am 103:1069–1084. https://doi.org/10.1785/0120120134

Kotha SR, Weatherill G, Bindi D, Cotton F (2020) A regionally-adaptable ground-motion model for shallow crustal earthquakes in Europe. Bull Earthq Eng 18:4091–4125. https://doi.org/10.1007/s10518-020-00869-1

Leynaud D, Jongmans D, Teerlynck H, Camelbeeck T (2000) Seismic hazard assessment in Belgium. Geol Belg 3:67–86

Martin C, Combes P, Secanell R, Lignon R, Firavanti A, Carbon D, Monge O, Grellet B (2002) Revision du zonage sismique de la France. Etude probabiliste. GEOTER.

McGarr A, Fletcher JB (2005) Development of ground-motion prediction equations relevant to shallow-mining-induced seismicity in the Trial Mountain area, Emery County, Utah. Bull Seismol Soc Am 95:31–47. https://doi.org/10.1785/0120040046

Mosca I, Sargeant S, Baptie B, Musson RMW, Pharaoh TC (2022) The 2020 national seismic hazard model for the United Kingdom. Bull Earthq Eng 20:633–675. https://doi.org/10.1007/s10518-021-01281-z

Pagani M, Monelli D, Weatherill G, Danciu L, Crowley H, Silva V, Henshaw P, Butler L, Nastasi M, Panzeri L, Simionato M, Vigano D (2014) OpenQuake Engine: An open hazard (and risk) software for the global earthquake model. Seismol Res Lett 85:692–702. https://doi.org/10.1785/0220130087

Rietbrock A, Strasser F, Edwards B (2013) A stochastic earthquake ground-motion prediction model for the United Kingdom. Bull Seismol Soc Am 103:57–77. https://doi.org/10.1785/0120110231

Rietbrock A, Edwards B (2019) Update of the UK stochastic ground motion model. In: SECED 2019 Conference. Greenwich, London, p. 10.

Scherbaum F, Cotton F, Smit P (2004) On the use of response spectral-reference data for the selection and ranking of ground-motion models for seismic-hazard analysis in regions of moderate seismicity: the case of rock motion. Bull Seismol Soc Am 94:2164–2185. https://doi.org/10.1785/0120030147

Scherbaum F, Delavaud E, Riggelsen C (2009) Model selection in seismic hazard analysis: an information-theoretic perspective. Bull Seismol Soc Am 99:3234–3247. https://doi.org/10.1785/0120080347

Toro GR (2002) Modification of the Toro et al. (1997) attenuation equations for large magnitudes and short distances.

Troch K (2018) Reforming mineral ownership and ensuring surface owners' rights: the gosselies disaster. Glob Environ 11:319–345. https://doi.org/10.3197/ge.2018.110206

Vanneste K, Vleminckx B, Verbeeck K, Camelbeeck T (2014) Development of seismic hazard maps for Belgium. In: Butenweg C, Kaiser D (Eds.) DGEB Workshop "Seismic Hazard Harmonisation in Europe (SHARE)." DGEB, Frankfurt a.M., Germany, pp. 61–68.

Verbeeck K, Vanneste K, Camelbeeck T (2009) Seismotectonic zones for probabilistic seismic-hazard assessment in Belgium. ONDRAF/NIRAS, Brussel

Villani M, Polidoro B, Mccully R, Ader T, Edwards B, Rietbrock A, Lubkowski Z, Courtney TJ, Walsh M (2019) A selection of GMPEs for the United Kingdom based on instrumental and macroseismic datasets. Bull Seismol Soc Am 109:1378–1400. https://doi.org/10.1785/0120180268

Wald DJ, Quitoriano V, Heaton TH, Kanamori H (1999) Relationships between peak ground acceleration, peak ground velocity, and modified mercalli intensity in California. Earthq Spectra 15:557–564

Wald DJ, Worden CB, Thompson EM, Hearne M (2022) ShakeMap operations, policies, and procedures. Earthq Spectra 38:756–777. https://doi.org/10.1177/87552930211030298

Weatherill G, Kotha SR, Cotton F (2020) A regionally-adaptable "scaled backbone" ground motion logic tree for shallow seismicity in Europe: application to the 2020 European seismic hazard model. Bull Earthq Eng 18:5087–5117. https://doi.org/10.1007/s10518-020-00899-9

Woessner J, Laurentiu D, Giardini D, Crowley H, Cotton F, Grünthal G, Valensise G, Arvidsson R, Basili R, Demircioglu MB, Hiemer S, Meletti C, Musson RW, Rovida AN, Sesetyan K, Stucchi M, Anastasiadis A, Akkar S, Engin Bal I, Barba S, Bard PY, Beauval C, Bolliger M, Bosse C, Bonjour C, Bungum H, Carafa M, Cameelbeeck T, Carvalho A, Campos-Costa A, Coelho E, Colombi M, D'amico V, Devoti R, Drouet S, Douglas J, Edwards B, Erdik M, Fäh D, Fonseca J, Fotopoulou S, Glavatovic B, Gómez Capera AA, Hauser J, Husson F, Kastelic V, Kästli P, Karatzetzou A, Kaviris G, Keller N, Kierulf HP, Kouskouna V, Krishnamurty R, Lang D, Lemoine A, Lindholm C, Makropoulos K, Manakou M, Marmureanu G, Martinelli F, Garcia Mayordomo J, Mihaljevic J, Monelli D, Garcia-Moreno D, Nemser E, Pagani M, Pinho R, Pisani AR, Pitilakis D, Pitilakis K, Poggi V, Radulian M, Riga E, Sandikkaya MA, Segou M, Siegert R, Silva V, Stromeyer D, Sousa L, Sørensen MB, Tellez-Arenas A, Vanneste K, Wahlstöm R, Weatherill G, Viganò D, Vilanova S, Yenier E, Zulfikar C, Adams J, Bommer JJ, Bonilla F, Faccioli E, Gülen L, Koller M, Pinto A, Pinto P, Papaioannou C, Peruzza L, Scherbaum F, Scotti O, Stirling M, Theodoulidis N, Wenk T, Zschau J (2015) The 2013 European Seismic Hazard Model: key components and results. Bull Earthq Eng 13:3553–3596. https://doi.org/10.1007/s10518-015-9795-1

Yenier E, Atkinson GM (2015) Regionally adjustable generic ground-motion prediction equation based on equivalent point-source simulations: application to central and Eastern North America. Bull Seismol Soc Am 105:1989–2009. https://doi.org/10.1785/0120140332

Zhao JX, Zhang J, Asano A, Ohno Y, Oouchi T, Takahashi T, Ogawa H, Irikura K, Thio HK, Somerville PG, Fukushima Y (2006) Attenuation relations of strong ground motion in japan using site classification based on predominant period. Bull Seismol Soc Am 96:898–913. https://doi.org/10.1785/0120050122